Astrochemical models

Jixing Ge (葛继兴)

collaborators: Diego Merdones, Jinhua He, Nantalia, Tie Liu, Shengli Qin, Mengyao Tang, Yaping Peng, Wang Zhong etc.

CASSACA

Personal website: https://sites.google.com/view/gejixing

gejixing666@gmail.com

Outline

Background

From interstellar clouds to star: the early stage

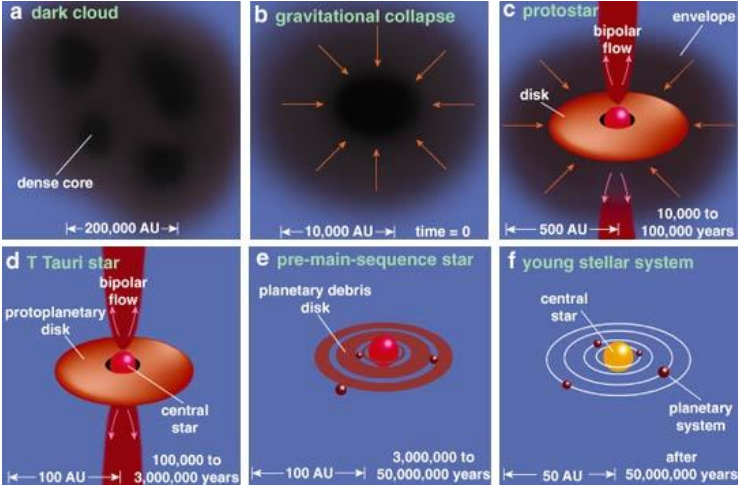

Raido observations towards molecular clouds & Hot cores.

mm & sub-mm of molecular lines

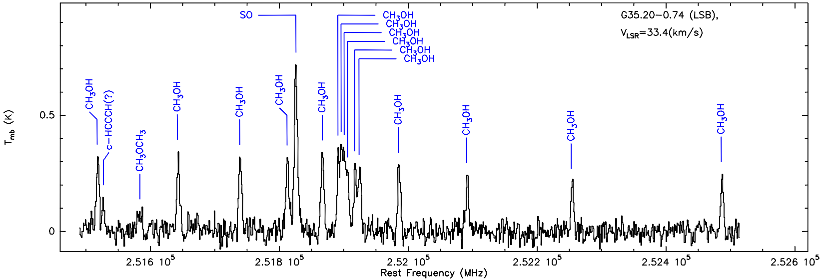

??

1. Molecular lines: CO, N_2H^+, OCS, HC_3N, CH_3OH etc
2. ↓Column density, abundance, excitation temperature and so on.

From radio observation to chemistry

Observations + Physics + chemistry

$\Downarrow$

1. $H_3{}^+ + N_2 \longrightarrow N_2H^+.$
2. $JCO \longrightarrow JHCO \longrightarrow JH_2CO \longrightarrow JCH_3OH$

$\Downarrow$

Chemical properties; evolution stage; chemical ages etc.

$\Downarrow$

New observations and models.

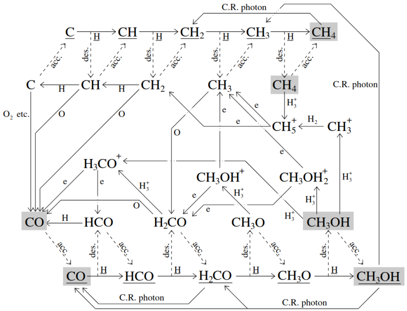

Figure from ?.

Evolution of physics and chemistry

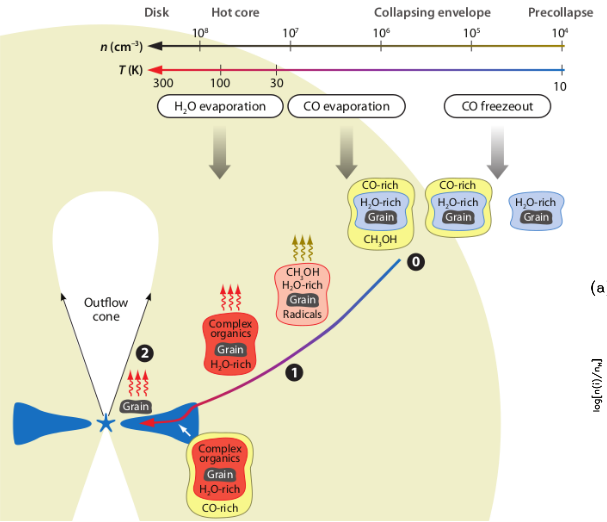

?

Hot core model:

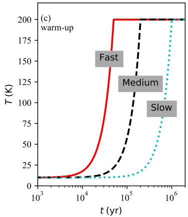

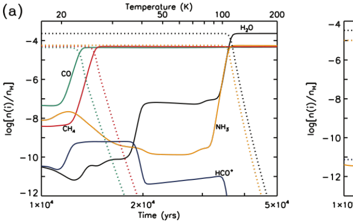

??

Astro-chemical models

Single-point chemical models

pure-gas

CO, N_2H^+ etc. E.g. **?, ?**

But H_2 and CH_3OH are mainly formed in solid-phase.

gas-grain (2-phase):

?, ?, ?

Species on dust grains should be buried in mantle.

gas-grain (3-phase):

?,?

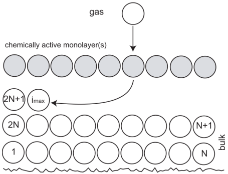

Vasyunina & Herbst tal., (2013)

Note: single-size dust grain is usually used.

Rate-equations

Gas:

$$\frac{dn_i}{dt} = \sum_{l,m} k_{lm} n_l n_m - n_i \sum_{i \neq l} k_l n_l + k_i^{des} n_i^s - k_i^{acc} n_i$$

Surface:

$$\frac{dn_i^s}{dt} = \sum_{l,m} k_{lm}^s n_l^s n_m^s - n_i^s \sum_{i \neq l} k_l^s n_l^s - k_i^{des} n_i^s + k_i^{acc} n_i$$

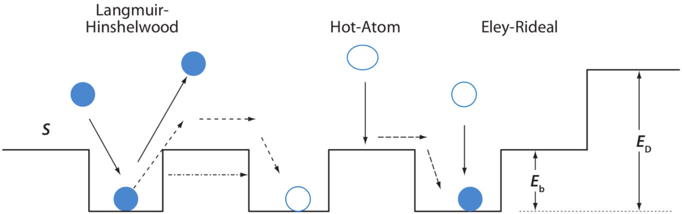

Figure 9

Three mechanisms for surface reactions on a regular grain surface. S is the sticking efficiency of a gas-phase species, E_D is the binding, or desorption, energy of the adsorbate to the surface, and E_b is the barrier from one site to an adjacent one.

?, ?

Benchmark of gas-grain code. (ggchem verse ALCHEMIC)

Physical parameters for five models from ?:

Model	T [K]	$n(H+2H_2)$ [cm^{-3}]	Av [mag]	χ[11]
TMC1	10	2(4)[12]	10	χ_0
HOT CORE	100	2(7)	10	χ_0
DISK1	11.4	5.41(8)	37.1	$428.3\chi_0$
DISK2	45.9	2.59(7)	1.94	$393.2\chi_0$
DISK3	55.2	3.67(6)	0.22	$353.5\chi_0$

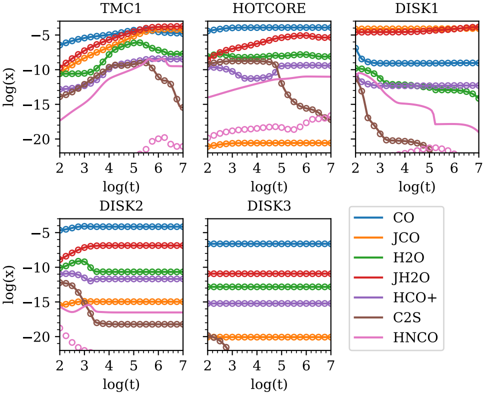

Figure 1: Lines: ggchem. Points: ALCHEMIC (?)

?:

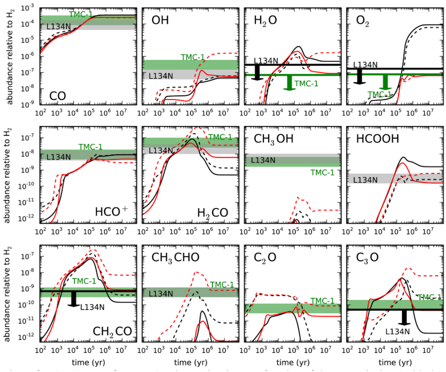

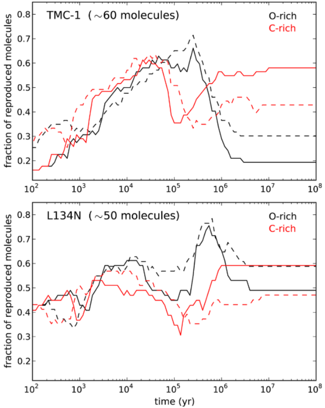

solid—KIDA, dashed—UMIST

Uncertainties

? + Monte Carlo method:
Assume a normal distributions of $\log(k_i)$ (k_i is reaction coefficient) with a standard deviation $\sigma_i = \log F_i$ (unertainty factor).
$\langle \log(X(t)) \rangle$—the averaged abundance is obtained at time t.
$\Delta \log(X) = \frac{1}{2}(\log X_{\max} - \log X_{\min})$
$\rightarrow$ 2σ symmetric Gaussian distribution.

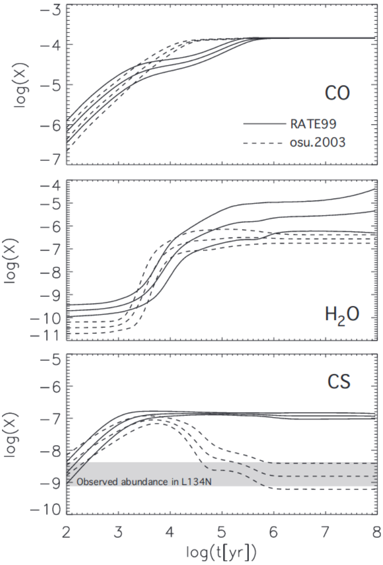

New chemical effects

Dust grain size distribution (1)

$$dn = c \times a^{-3.5} da \text{ (?); ?}$$

?:

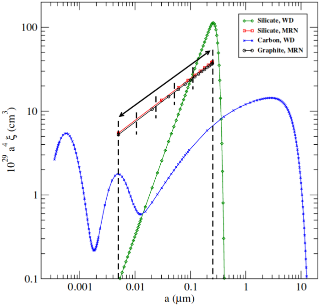

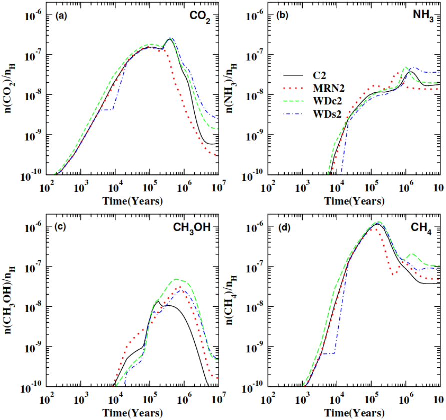

Dust size distribution introduces some effects on abundance, but not big.

Dust grain size distribution (2)

- HY(from MHD calculation)/ or WD+$T_d(i)$? $\Rightarrow$ different areal densities:

	DC[a]			CNM[b]	
a (cm)	$n_d(a)$ (cm^{-3})	$T_d(a)$ (K)	a (cm)	$n_d(a)$ (cm^{-3})	$T_d(a)$ (K)
1.13×10^{-6}	1.17×10^{-7}	9.1	1.15×10^{-6}	3.33×10^{-9}	17.9
1.37×10^{-6}	7.87×10^{-8}	9.1	1.55×10^{-6}	1.84×10^{-9}	17.9
1.57×10^{-6}	5.96×10^{-8}	9.1	2.13×10^{-6}	9.78×10^{-10}	17.8
1.81×10^{-6}	4.49×10^{-8}	9.1	2.97×10^{-6}	5.01×10^{-10}	17.5
2.28×10^{-6}	2.85×10^{-8}	9.1	4.23×10^{-6}	2.48×10^{-10}	16.9
3.18×10^{-6}	1.47×10^{-8}	9.1	6.11×10^{-6}	1.19×10^{-10}	16.2
4.75×10^{-6}	6.54×10^{-9}	9.1	8.96×10^{-6}	5.53×10^{-11}	15.6
7.90×10^{-6}	2.37×10^{-9}	9.1	1.32×10^{-5}	2.54×10^{-11}	15.2
1.57×10^{-5}	5.97×10^{-10}	9.1	1.96×10^{-5}	1.16×10^{-11}	14.9

Notes. [a]Hirashita & Yan (2009); [b]Weingartner & Draine (2001).

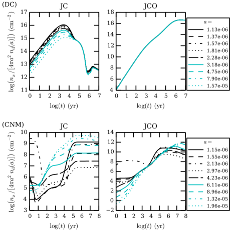

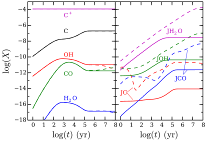

models

areal density

abundance in CNM

- MRN + $T_d(i) \propto a_{\mathrm{eff}}^{-1/6}(i)$ $\Rightarrow$ effects in mantle ?:

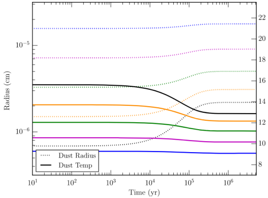

(c) Model 5G_T10_DIST

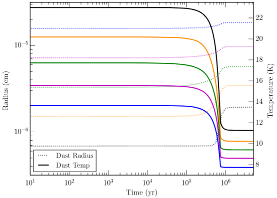

(d) Model 5G_COLL

Dust temperature as function of radii does affect the mantle composition.

Dust grain size distribution (3)

- ?: Monte Carlo + Cooling & heating of dust grains

Stochastic heating ⇐ low energy (infrared wavelength) + high energy (cosmic-ray induced secondary FUV) photons.

- gas-grain + 5bins + HY/MRN
- Grain coagulation can affect certain gas-phase species, such as CO2 and N2H+, in the cold core environments, which can be attributed to the volatile precursors originating from the small grains with temperature fluctuations;
- Grains with radii around 4.6×10^{-3} μm contribute most to the production of COMs on dust grains under cold core conditions, while few species can be formed on even smaller grains with radii less than 2×10^{-3} μm;
- COMs formed on stochastically heated grains could help explain the observed abundances of gas-phase COMs in cold cores.

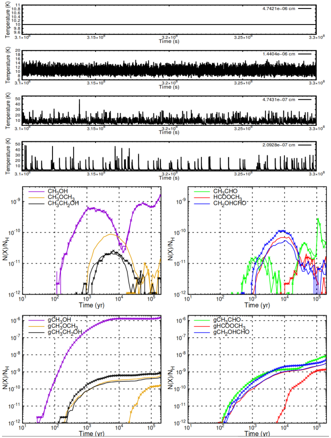

line with cross:— M3, line— M4

Non-thermal desorption(1)

- The thermal desoprtion is not enough to produce high abundances of COMs at 10 K.

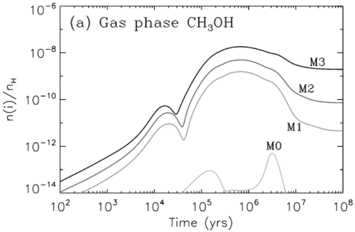

- $P = \left[1 - \frac{E_D}{E_{reac}}\right]^{s-1}, f = \frac{aP}{1+aP}$, ? + Rice-Ramsperger-Kessel (RRK) theory[a].
  $a = 0.0$(M0), 0.01(M1), 0.03(M2), 1.0(M3). L134N and TMC-1CP.

- Efficiency $CD = \exp(-\frac{E_b \cdot s}{\epsilon \Delta H}), \epsilon = \left(\frac{m-M}{m+M}\right)^2$?:

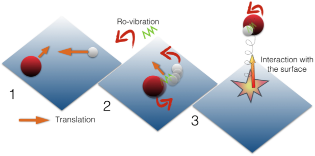

Fig. 4. Illustration of the chemical desorption process. After an initial meeting (1), the molecule is highly excited; (2) and converts a fraction of its energy into vertical motion through interaction with the surface (3).

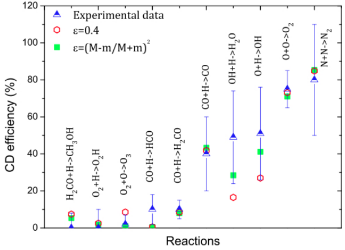

---

[a] s is the number of vibrational modes in the molecule/surface-bond system

Non-thermal desorption(2)

- ?: dust size-dependent CR heating

$$k_{crd} = f(T_{max}(i))k_{evap}(i, T_{max}(i))$$

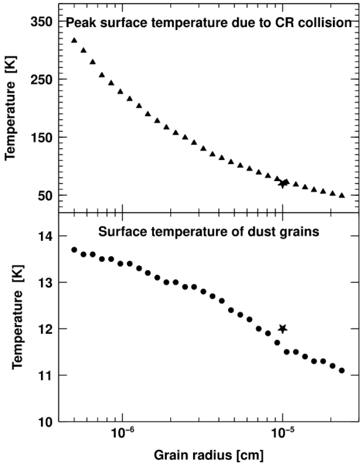

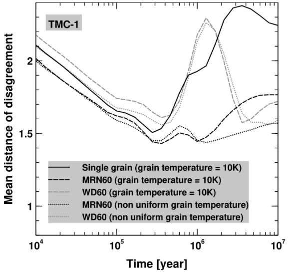

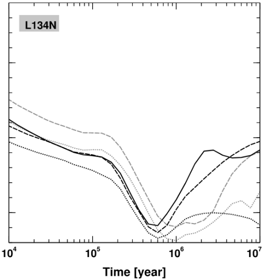

Hightlight the role of small grains.

Non-thermal desorption(3)

- sputtering of grain mantles induced by cosmic rays **?**

$k = (\zeta/3 \times 10^{-17}) Y_{\rm eff} \pi a^2 / N_{\rm site}$, $Y_{\rm eff} = Y^{\infty}(1 - e^{-(n_{\rm layers}/\beta)^{\gamma}})$ where $Y_{\rm eff}$ is the efficiency of desorption integrated over a cosmicray spectral distribution. Y^{∞} is the sputtering yield for thick ices and β, γ are two parameters associated to nature of the ice.

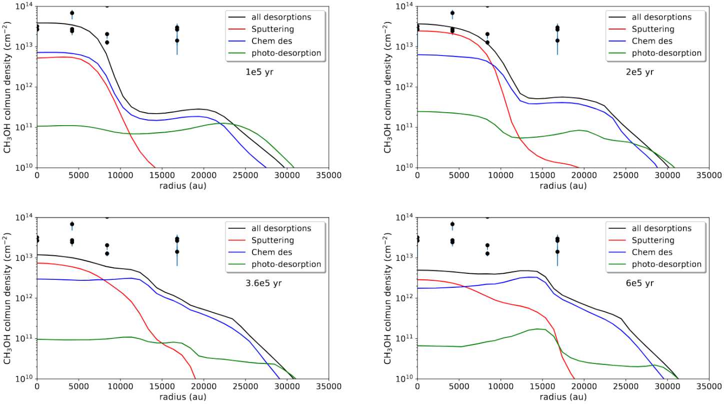

Black: all desorption, red: sputtering; blue: chem res; green: photo-des

New reactions of S-bearing species

- **?**: enhanced network + cosmic value of S ($\sim 1.5 \times 10^{-5}$):

e.g. $HCS^+ + NH_2 \longrightarrow H + H_2NCS^+ \xrightarrow{e^{-1}} HNCS/HSCN + H$

the reservoir of sulphur $\Rightarrow$ atomic sulphur in the gas phase or HS and H_2S in icy grain bulks.

Model	$n(S)_{ini}$[a]
1	8(− 8)
2	5(− 7)
3	5(− 6)
4	1.5(− 5)

[a] $a(b)$ stands for $a \times 10^b$.

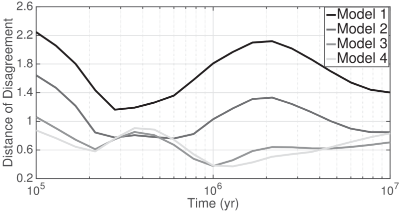

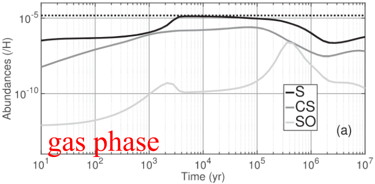

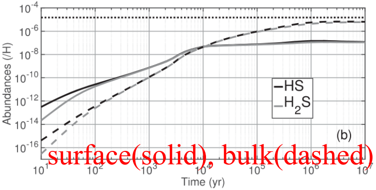

New reactions of S-bearing species

- ?: enhanced network + cosmic value of S + multiple stages (Diffuse + Translucent + Dense)

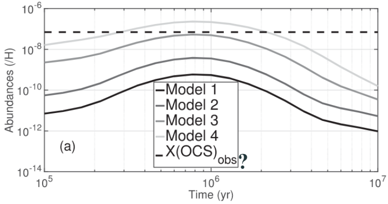

Abundance ratios: OCS_{ice} vs. CO_{ice}.

Environment	Abundance (%)
W33A	5
AFGL 989	0.8
Mon R2 IRS2	0.65
AFGL 961E	<1
AFGL 490	<2.6
NGC 2024 IRS 2	<0.8
OMC 2 IRS 3	<1.6
Elias 16	<0.8
$n = 10^4$ cm^{-3}	0.7
$t = 2$ Myr	
$n = 10^5$ cm^{-3}	4
$t = 0.3$ Myr	
$n = 10^6$ cm^{-3}	5
$t = 0.03$ Myr	

$X(OCS_{ice}) \sim 10^{-8}$ (?).

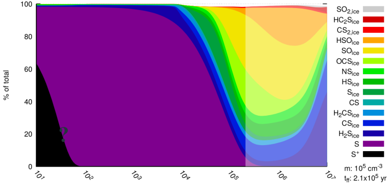

$X(OCS_{ice}) \sim 10^{-8}$ (?).

Percentages (?).

PAHs in dark clouds. Observations.

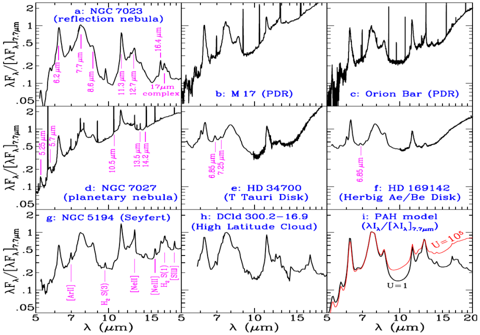

(Li+2020)

- Abundance $\sim 10^{-7}$ from ratio of DCO+/HCO+ (?)

- PAH database:

https://www.dsf.unica.it/~gmalloci/pahs/pahs.html

NIST: https://webbook.nist.gov/chemistry/

PAHdb: https://www.astrochemistry.org/pahdb/

PAHs in dark clouds. Wakelam et al., (2008)

- PAH chemistry & models (?)

$3.8 \rightarrow 6\text{Å}, \Rightarrow a = 4\text{Å}, N_C = 460(a/10\text{Å})^3 = 30, X(\text{PAH}) = 3.07 \times 10^{-7}$.

Radiative electron attachment: $\text{PAH} + e^- \longrightarrow \text{PAH}^- + h\nu$, $k_e = 10^{-7} N_C^{3/4}$

Charge exchange:

$\text{PAH}^- + X^+ \longrightarrow \text{PAH} + X$

$\text{PAH}^- + X^+ \longrightarrow \text{PAH} + X' + H$, if the positive ion contains Hydrogen

$k = \pi a^2 \langle \nu_0 \rangle \left(1 + \frac{e^2}{a k_B T}\right)$ where $\langle \nu_0 \rangle = \sqrt{\frac{8 k_B T}{\pi \mu}}$ is the mean relative velocity.

$\text{PAH}^- + h\nu \longrightarrow \text{PAH} + e^-$

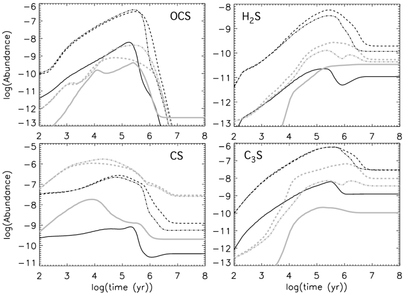

Enhanced abundances and agreements.

PAHs in dark clouds. Ge et al., (2020b)

- Ge et al., (2020b)： PAHs chemisty.

We introduced PAHs into a 3-phase model and found that:

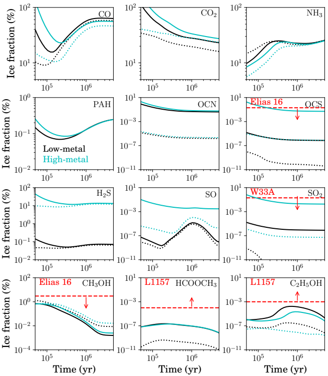

high-metal， low metal.

The model with PAH produces comparable solid-phase OCS abundance.

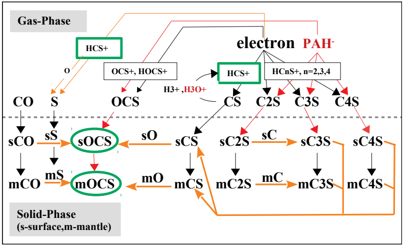

This is consistent with that of ? and ? by enhancing reaction network.

PAHs in dark clouds. Ge et al., (2020b)

The model with PAHs produces comparable results to that in comet 67P/Churyumov-Gerasimenko (67P/C-G):

Species	Model	Model+PAHs	comet 67P/C-G
H_2S	1.24×10^{-1}	1.36×10^{-1}	$(1.10 \pm 0.05) \times 10^{-2a}$
OCS	8.23×10^{-9}	5.37×10^{-4}	$(4.08 \pm 0.09) \times 10^{-4a}$
SO	3.34×10^{-7}	3.38×10^{-5}	$(7.10 \pm 1.10) \times 10^{-4a}$
SO_2	5.56×10^{-10}	1.94×10^{-4}	$(1.27 \pm 0.03) \times 10^{-5a}$
S_2	3.90×10^{-6}	3.25×10^{-5}	$(1.97 \pm 0.35) \times 10^{-5a}$
H_2CS	8.65×10^{-5}	2.70×10^{-4}	$(2.67 \pm 0.75) \times 10^{-6a}$
H_2S_2	7.72×10^{-7}	3.63×10^{-5}	$< 6.04 \times 10^{-6b}$
HS_2	7.96×10^{-7}	8.46×10^{-6}	$< 1.06 \times 10^{-6b}$
PO	1.44×10^{-6}	4.49×10^{-5}	$\sim 1.10 \times 10^{-4b}$
PN	2.07×10^{-5}	2.13×10^{-4}	$< 1.10 \times 10^{-5b}$
HCl	7.78×10^{-6}	2.54×10^{-4}	$\sim 1.40 \times 10^{-4b}$

a: Data from (**??**); b: Data from **?** and references therein.

Three-dimensional projection effects on chemistry in a Planck cold clump G224.4-0.6

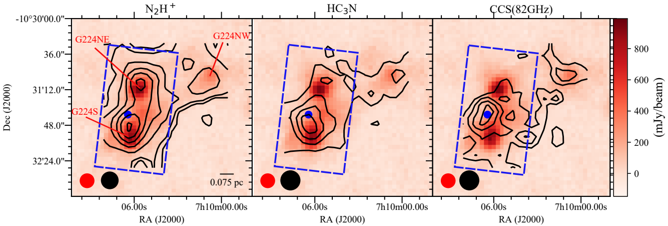

Using the Plummer-like 1-D profile, four cores can be used to reproduce H2 column density map:

Plummer-like radial density function for spherical dense core:

$$n(r) = \frac{n_c}{[1+(r/r_c)^2]^{p/2}} + n_b$$

n_c: center density,
n_b: background
r_c: inner flat region length
p: power-law index

(1)

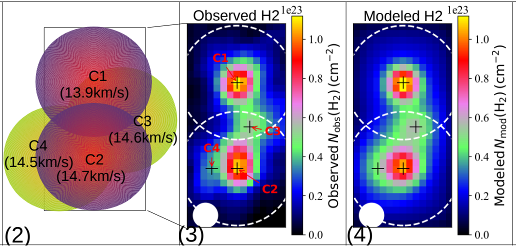

?

Three-dimensional projection effects on chemistry in a Planck cold clump G224.4-0.6

The molecular distributions can be reproduced at a given age:

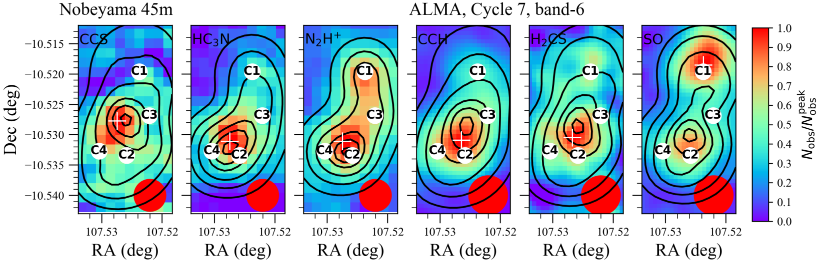

Left: comparison with previous observations.

Right: comparison with new ALMA Cycle-7 observations.

The projection effects of the four cores can be use to reproduce molecular distributions. This provides a new method to explore 3-D structure of interstellar clouds using molecular lines (**?**)

Outlook

Comparative studies of dark clouds, hot molecular cores and molecular outflows will provide useful information to the ice composition on dust grains and to find the key reactions to the origin of life from views of the formation of organic molecules.

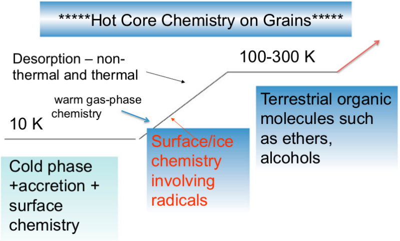

up to a few 1000 K in outflows

Improved Models: **GGCHEM** for DC and HMC, **UCLCHEM** and **mhd_vode** for shock chemsitry.

High-resolution Observations: ALMA, APEX etc.

Thank you!

References

Acharyya K., Hassel G. E., Herbst E., 2011, ApJ, 732, 73

Agúndez M., Wakelam V., 2013, Chemical Reviews, 113, 8710

Calmonte U., et al., 2016, MNRAS, 462, S253

Caselli P., Hasegawa T. I., Herbst E., 1998, ApJ, 495, 309

Chen L.-F., Chang Q., Wang Y., Li D., 2022, Complex Organic Molecules Formation in Cold Cores on Stochastically Heated Grains, `http://arxiv.org/abs/2209.05190`

Drozdovskaya M. N., van Dishoeck E. F., Rubin M., Jørgensen J. K., Altwegg K., 2019, MNRAS, 490, 50

Garrod R. T., 2008, A&A, 491, 239

Garrod R. T., Herbst E., 2006, A&A, 457, 927

Garrod R. T., Wakelam V., Herbst E., 2007, A&A, 467, 1103

Garrod R. T., Vasyunin A. I., Semenov D. A., Wiebe D. S., Henning T., 2009, ApJL, 700, L43

Ge J. X., He J. H., Chen X., Takahashi S., 2014, MNRAS, 445, 1170

Ge J. X., He J. H., Yan H. R., 2016a, MNRAS, 455, 3570

Ge J. X., He J. H., Li A., 2016b, MNRAS, 460, L50

Ge J. X., et al., 2020, ApJ, 891, 36

Gillespie D. T., 1976, Journal of Computational Physics, 22, 403

Hasegawa T. I., Herbst E., 1993a, MNRAS, 261, 83

Hasegawa T. I., Herbst E., 1993b, MNRAS, 263, 589

Hasegawa T. I., Herbst E., Leung C. M., 1992, ApJS, 82, 167

He J. H., Takahashi S., Chen X., 2012, ApJS, 202, 1

Herbst E., van Dishoeck E. F., 2009, ARA&A, 47, 427

Iqbal W., Wakelam V., 2018, A&A, 615, A20

Laas J. C., Caselli P., 2019, Astron. Astrophys., 624, A108

Lepp S., Dalgarno A., 1988, ApJ, 324, 553

Mathis J. S., Rumpl W., Nordsieck K. H., 1977, ApJ, 217, 425

McElroy D., Walsh C., Markwick A. J., Cordiner M. A., Smith K., Millar T. J., 2013, A&A, 550, A36

Minissale M., Dulieu F., Cazaux S., Hocuk S., 2016, A&A, 585, A24

Pauly T., Garrod R. T., 2016, ApJ, 817, 146

Ruaud M., Wakelam V., Hersant F., 2016, MNRAS, 459, 3756

Semenov D., et al., 2010, A&A, 522, A42

Shingledecker C. N., Lamberts T., Laas J. C., Vasyunin A., Herbst E., Kästner J., Caselli P., 2020, ApJ, 888, 52

Tang M., et al., 2018, ApJ, 856, 141

Tang M., et al., 2019, ApJ, 887, 243

Vasyunin A. I., Semenov D. A., Wiebe D. S., Henning T., 2009, ApJ, 691, 1459

Vidal T. H. G., Loison J.-C., Jaziri A. Y., Ruaud M., Gratier P., Wakelam V., 2017, MNRAS, 469, 435

Wakelam V., Herbst E., 2008, ApJ, 680, 371

Wakelam V., Herbst E., Selsis F., 2006, A&A, 451, 551

Wakelam V., Dartois E., Chabot M., Spezzano S., Navarro-Almaida D., Loison J.-C., Fuente A., 2021, A&A, 652, A63

Weingartner J. C., Draine B. T., 2001, ApJ, 548, 296